High-quality graphene on single crystal Ir(1 1 1) films on Si(1 1 1) wafers: Synthesis and multi-spectroscopic characterization

ARTICLE *in* CARBON · SEPTEMBER 2014

Impact Factor: 6.2 · DOI: 10.1016/j.carbon.2014.09.045

CARBON 81 (2015) 167–173

Available at www.sciencedirect.com

ScienceDirect

journal homepage: www.elsevier.com/locate/carbon

High-quality graphene on single crystal Ir(111) films on Si(111) wafers: Synthesis and multi-spectroscopic characterization

C. Struzzi [a,*], N.I. Verbitskiy [b,c,d], A.V. Fedorov [d,e,f], A. Nefedov [g], O. Frank [h], M. Kalbac [h], G. Di Santo [a,i], M. Panighel [a,j], A. Goldoni [a,i], J. Gärtner [k], W. Weber [k], M. Weinl [l], M. Schreck [l], Ch. Wöll [g], H. Sachdev [m], A. Grüneis [d,e], L. Petaccia [a,*]

[a] Elettra Sincrotrone Trieste, Strada Statale 14 km 163.5, 34149 Trieste, Italy
[b] Faculty of Physics, University of Vienna, Strudlhofgasse 4, A-1090 Vienna, Austria
[c] Department of Materials Science, Moscow State University, Leniniskiye Gory 1/3, 119992 Moscow, Russia
[d] II. Physikalisches Institut, Universität zu Köln, Zülpicher Straße 77, 50937 Köln, Germany
[e] IFW Dresden, P.O. Box 270116, D-01171 Dresden, Germany
[f] St. Petersburg State University, St. Petersburg 198504, Russia
[g] Institute of Functional Interfaces, Karlsruhe Institute of Technology (KIT), 76344 Eggenstein-Leopoldshafen, Germany
[h] J. Heyrovsky Institute of Physical Chemistry of the AS CR, v.v.i., Dolejskova 2155/3, CZ-182 23 Prague 8, Czech Republic
[i] INSTM – Elettra, Strada Statale 14 km 163.5, 34149 Trieste, Italy
[j] Department of Physics, University of Trieste, via Valerio 2, 34100 Trieste, Italy
[k] NaMLab gGmbH, Noethnitzer Str. 64, 01187 Dresden, Germany
[l] Institut für Physik, Universität Augsburg, D-86135 Augsburg, Germany
[m] Max Planck Institut für Polymerforschung, Ackermannweg 10, D-55128 Mainz, Germany

ARTICLE INFO

Article history:
Received 7 May 2014
Accepted 16 September 2014
Available online 23 September 2014

ABSTRACT

The characterization of graphene by electron and optical spectroscopy is well established and has led to numerous breakthroughs in material science. Yet, it is interesting to note that these characterization methods are almost never carried out on the same sample, i.e., electron spectroscopy uses epitaxial graphene while optical spectroscopy relies on cleaved graphene flakes. In order to bring coherence and convergence to this branch, a universal and easy-to-prepare substrate is needed. Here we suggest that chemical vapour deposition (CVD) grown graphene on thin monocrystalline Ir(111) films, which are grown heteroepitaxially on Si(111) wafers with an yttria stabilized zirconia (YSZ) buffer layer, perfectly meets these needs. We investigate graphene prepared in this way by low-energy electron diffraction (LEED), X-ray photoelectron spectroscopy (XPS), near edge X-ray absorption fine structure (NEXAFS) spectroscopy, angle-resolved photoemission spectroscopy (ARPES), resonance Raman spectroscopy, and scanning tunnelling microscopy (STM). Our results highlight the excellent crystalline quality of graphene, comparable to graphene prepared on Ir(111) bulk single crystals. This synthesis route allows for large-area, inexpensive

* *Corresponding authors:* Fax: +39 0403758029 (L. Petaccia).
E-mail addresses: claudia.struzzi@gmail.com (C. Struzzi), luca.petaccia@elettra.eu (L. Petaccia).
http://dx.doi.org/10.1016/j.carbon.2014.09.045

growth on standardized disposable substrates, suitable for both optical and electron spectroscopic characterization, which meets the needs of many researchers in the field.

1. Introduction

Recent research efforts in carbon nanoscience are directed towards efficient applications of graphene as a base for modern nanoelectronic devices, like high frequency transistors and organic solar cells [1–3]. Nevertheless, all of such devices are present only as prototypes and have not been mass-produced. Efficient growth of high-quality graphene *via* chemical vapour deposition (CVD) on transition metals (TMs) makes this approach a prominent candidate for graphene mass-production. In many cases, epitaxial growth enables a production of macroscopic samples and it has been shown for several systems that epitaxial graphene can also be removed from its substrate, typically by chemical etching, and transferred to an arbitrary support, especially insulating ones [4–9]. These are fundamental steps for device fabrication and it is important to expand more and more the variety of fabrication routes to meet specific needs. In case of TMs there are two scenarios of graphene-substrate interaction: (i) strong bonding (e.g., Ni, Ru) with hybridization of π graphene electrons with TM bands and high perturbation of graphene band structure [10–14]; (ii) weak bonding (e.g., Au, Pt, Ir), when graphene is quasi-freestanding [15–17]. Graphene could form lattice-mismatched systems, or so called nanomeshes, with some TMs like Ir and Ru, that are also interesting in applications, due to the possibility of ordered clusters formation and diffraction effects in the electronic structure [18]. In the case of Ir, graphene can be prepared with an exceptionally high structural quality and as a single layer. The solubility of carbon in iridium is insignificant at suitable graphene formation temperatures. Thereby, graphene growth can be controlled by hydrocarbon supply and self-limited by the availability of uncovered Ir(111) area, which shrinks during growth.

However, crystalline bulk Ir(111) substrates are costly and it would be much more convenient to use, and later eventually dissolve, only a metal monocrystalline thin film. High crystal quality and low-cost thin film of Ir(111) can be grown on Si(111) with an yttria-stabilized zirconia (YSZ) buffer layers [19–21]. Recently, graphene of high structural quality has been prepared on this new substrate and characterized by scanning tunnelling microscopy (STM) and low energy electron diffraction (LEED) [22,23]. On the other hand, no information on the electronic and vibrational properties has been reported yet.

In this work we carry out such a characterisation using a multimode spectroscopic and microscopic approach, combining core-level (XPS) and angle-resolved (ARPES) photoemission, near-edge X-ray absorption (NEXAFS), and Raman spectroscopies. In order to check the structural quality of the synthesized graphene, LEED and STM have also been performed. The information provided by these complementary techniques allows us to further show that this fabrication process yields air-stable graphene of extraordinary quality so that several demanding and not necessarily compatible experimental techniques can be employed on the same sample. Furthermore, this fabrication technique can potentially be scaled towards larger output and, using Si wafers, can be more easily implemented into standard Si technology than processes based on other supports.

2. Experimental

2.1. Sample preparation

Epitaxial YSZ films (thickness 40–150 nm) on 4 in. Si (111) wafers were prepared by pulsed laser deposition using a KrF excimer laser (pulse duration: 25 ns, pulse energy: 850 mJ) at about 970 K. Two different cylindrical ablation targets of ZrO_2 containing 21.4 mol% or 6.5 mol% of $YO_{1.5}$, respectively, were used [19,24,25]. Iridium films with a thickness of 150 or 500 nm were then evaporated on top, keeping the substrate temperature at about 920 ± 50 K. During the first 20 nm a low deposition rate of 0.004 nm/s facilitated a good epitaxial alignment. For the rest of the Ir film deposition the rate was increased to 0.02 nm/s [19,25]. The Ir(111) film substrate was cleaned in ultra-high vacuum (UHV) via Ar^+ ion sputtering treatment and annealing cycles up to 1150 ± 50 K. A clear (1 × 1) hexagonal diffraction pattern was observed by LEED and the characteristic electronic bands of the Ir(111) surface was measured by ARPES (see Supplementary Data). Graphene was grown by CVD, by heating the substrate at about 1200 ± 50 K and feeding the precursor ethanol gas into the chamber at a partial pressure of about 5×10^{-7} mbar for 5 min. Comparative experiment with propylene as a precursor yields similar results (Supplementary Data). Using lower and higher temperatures during the CVD growth provides graphene of poorer electronic and structural quality while at temperatures higher than about 1300 K the surface starts to deteriorate visibly. The sample temperature was measured by an infrared pyrometer with emissivity set to 0.5.

2.2. Sample characterization

The XPS and NEXAFS measurements were carried out at the HESGM beamline of BESSY-II synchrotron in Berlin [26]. For XPS spectra a photon energy of 330 eV was used to excite electrons from C1s and Ir4f core levels, whereas the absorption spectra were acquired in total yield mode across the C-K edge at different X-ray incidence angles with respect to the sample surface plane. NEXAFS experiments allow probing the sp^2 fraction and planarity of graphene. When the electric field vector of the light is perpendicular to the graphene sheet, transitions from the C1s core level to the π^* band are allowed, while for the electric field vector completely lying in the graphene sheet, transitions to the σ^* bands are induced. This gives us the possibility to probe the planarity of the

synthesized graphene and rule out the presence of amorphous carbon [27].

ARPES measurements were carried out at the BaDElPh beamline [28] of Elettra synchrotron in Trieste. Using both horizontal (p) and vertical (s) polarized radiation and a photon energy of 34 eV we have followed the dispersion of π and σ states of graphene in the valence band by scanning the Brillouin Zone (BZ) along the high symmetry directions and got access to the details of regions of interest, as the Dirac cone. The overall energy and angular resolution was set to 100 meV and less than 0.3°, respectively.

Raman spectra were measured at microRaman (LabRAM HR spectrometer, Horiba Jobin–Yvon) with microscope Olympus BX under ambient conditions. The spectra were excited by an Ar^+–Kr^+ laser operating at 488 nm (2.54 eV) wavelength. The laser power at the sample under a 100× objective was kept at 1 mW. A diffraction grating of 600 grooves/mm was used giving a point-to-point spectral resolution of 1.8 cm^{-1} on a back-illuminated Peltier-cooled charged coupled device (CCD) detector. No analyser for selecting the polarization direction of the scattered light was used. The accumulation time for each spectrum was 20 min. The Raman spectrometer was calibrated before each set of measurements using the F_{1g} line of Si at 520.2 cm^{-1} as a reference. Raman D, G, and 2D bands were used to access the number of graphene layers, the defects concentrations, and the strain [29].

Scanning tunnelling microscopy (STM) imaging was performed at the Micro&Nano Carbon Laboratory at Elettra equipped with an Omicron® UHV RT AFM–STM machine with ApeResearch® electronics, in a base pressure better than 10^{-9} mbar. The bias voltage refers to the sample, and the images were recorded in constant current mode. Moderate filtering was applied for noise reduction. A chemically etched W tip was used as the STM probe. The tip was annealed at 700 K by electron bombardment in UHV to remove the native oxide. The STM data were processed with the software Gwyddion (http://gwyddion.net). The morphological characterisation at atomic resolution is conclusive for evaluating the quality of the surface and for the determination of the superstructure.

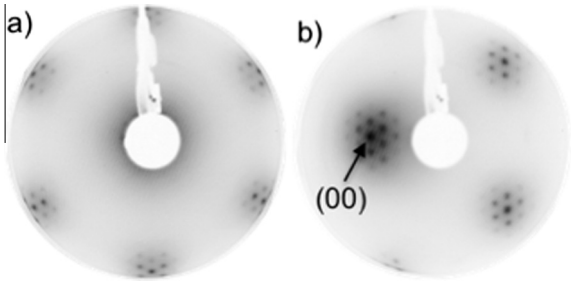

Fig. 1 – LEED pattern of graphene on Ir(1 1 1) film: (a) electron beam energy *E* = 75 eV and incidence angle of 0° from the sample surface normal; (b) electron beam energy *E* = 61 eV and incidence angle of about 10° off, in order to see also the (0 0) diffraction spot. The horizontal axis is parallel to the ΓK high symmetry direction. After CVD treatments, the integer order spots of the Ir substrate (see Supplementary Data) are surrounded by Moiré spots, arising from the lattice mismatch between graphene and iridium.

The sample synthesis for photoemission, LEED, and absorption measurements was performed *in situ*, while for the STM and Raman characterizations samples were exposed to air. Prior to the STM measurement, samples were annealed in UHV at 770 K in order to desorb air pollutant related species. All measurements were performed at room temperature.

3. Results and discussion

In Fig. 1 the LEED patterns of the as grown graphene are shown. The diffraction image in (a) has been acquired by setting the electron beam to an energy of 75 eV and an incidence angle of 0° from the sample surface normal. In (b), instead, the energy was set at 61 eV and the incidence angle was about 10° off the normal. The latter geometry facilitates the observation of the (0 0) diffraction spot. The patterns exhibit the well known Moiré superstructure of the R0 phase, corresponding to a lattice-aligned graphene layer without additional domains [30].

The XPS spectra of Ir4f and C1s core levels are shown in Fig. 2(a) and (b), respectively. The photoemission binding energy has been calibrated with respect to $Ir4f_{7/2}$ bulk state at 60.8 eV. For all the XPS spectra, a Shirley background has been subtracted and a Doniach–Sunjic (DS) lineshape analysis has been performed, by convoluting it with a Gaussian lineshape, representing the overall experimental energy resolution of 0.1 eV. The absence of oxygen 1s core level confirms the cleanness of the graphene. The fit to the iridium related spectrum has been performed by using four Doniach–Sunjic lineshapes: $4f_{7/2}$ and $4f_{5/2}$ states are both characterised by double peaks attributed to the bulk and surface components. Together with LEED of the pristine Ir film (see Supplementary Data), this is a signature of a clean and ordered surface structure of the film, whose surface quality is comparable to the one of bulk Ir(1 1 1) [14].

C1s spectrum reported in Fig. 2(b) shows a single component along with the DS fit. We extract the location of the peak at 284.27 ± 0.05 eV, an half width at half maximum (HWHM) of 0.21 ± 0.05 eV, and an asymmetry parameter α of 0.09, obtaining similar values than those of graphene grown on bulk Ir(1 1 1) single crystal [18].

In Fig. 2(c), the NEXFAS spectra are plotted. The spectra clearly show the C1s – π^* transition at 285.95 eV and the C1s – σ^* transition above 292 eV. Moreover, a low intensity band at the pre-edge can also be seen. It is a characteristic spectral feature of the unoccupied density of state (DOS) of single-layer graphene, as previously predicted by local-density approximation calculations [31] and shown by a detailed NEXAFS investigation of graphene [27]. The angle dependence proves that the π^* peak has a minimum in intensity for normal incidence. This is in agreement with the NEXAFS experiments performed on graphite [32] and previous measurements on graphene [27], confirming the high quality of well ordered planar graphene prepared on heteroepitaxial Ir films and demonstrating the lack of strong chemical bonding of graphene with underlying Ir growth substrate.

The spectrum of Fig. 3(a) displays electronic band structure along ΓM and ΓK high symmetry directions. Both the π and σ bands of graphene are clearly visible together with the Ir bands [33].

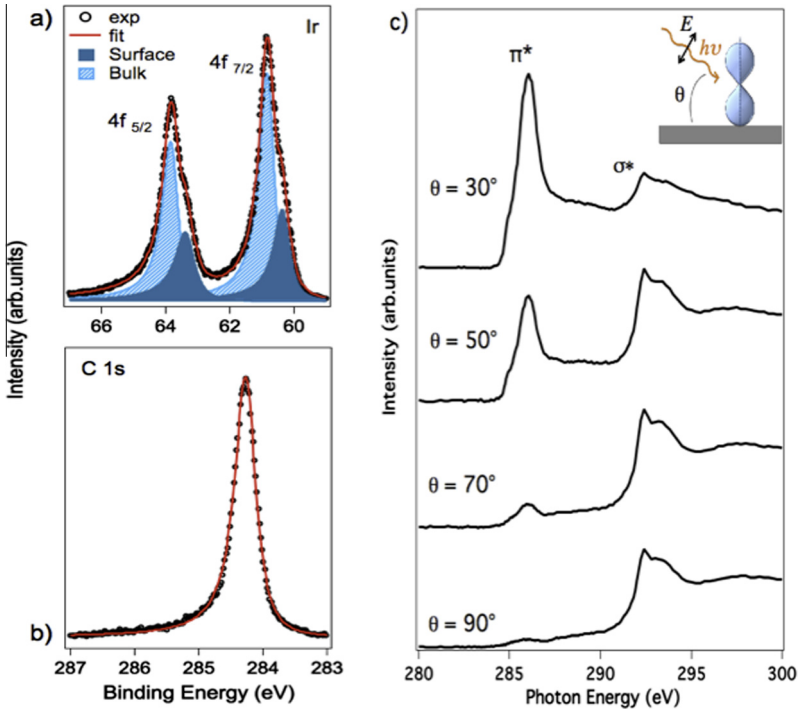

Fig. 2 – (a and b) XPS acquired by following Ir4f signals and C1s after graphene growth. The red solid lines represent the fits to the experimental data (black circles). (c) NEXAFS measurement from Carbon K-edge at different incidence angles (see inset) from grazing ($\theta = 30°$) to normal incidence ($\theta = 90°$) geometry. The corresponding electric field *E* of the light is almost out of the surface plane or in the surface plane, respectively. (A color version of this figure can be viewed online.)

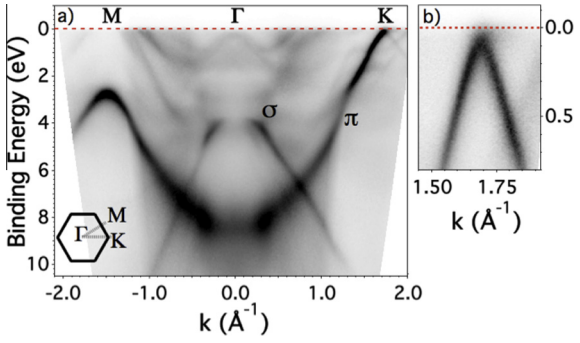

Fig. 3 – (a) ARPES measurement of graphene on Ir/YSZ/Si along ΓM and ΓK high symmetry directions. The inset depicts a sketch of the BZ of graphene. (b) Detail of Dirac cone along the ΓKM high symmetry direction, the dotted line at zero binding energy is the Fermi level. (A color version of this figure can be viewed online.)

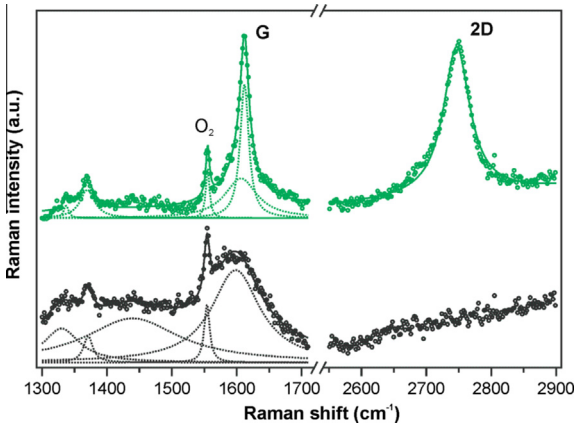

Fig. 4 – Raman spectra of graphene grown on Ir/YSZ/Si (top spectrum, green) and of a zone of iridium surface covered by the tantalum clip during graphene growth (bottom spectrum, black). The experimental spectra (points) were decomposed using Lorentzian lineshapes (dotted lines) with the solid line representing the sum of the individual Lorentzian components. (A color version of this figure can be viewed online.)

The replica of the π band is present and reclined around $k = 1.4$ Å^{-1} at 1 eV in binding energy, along ΓK direction the π band is perturbed by another replica placed at 3 eV [33], where it hybridizes also with the bands of the underlying substrate. The presence of these replicas is in accordance with the results derived from LEED reported in Fig. 1: they are related to Moiré superstructure as already studied in the literature [33–35], confirming the overall quality of graphene, which is comparable to that grown on bulk Ir single crystal [33].

The details of the Dirac cone are presented in Fig. 3(b), summing up the data acquired in horizontal (p) and vertical (s) polarization [36,37] in order to get information about the location of the Dirac point. Within the experimental resolutions, it is placed at the Fermi level and at 1.7 Å^{-1} proving that

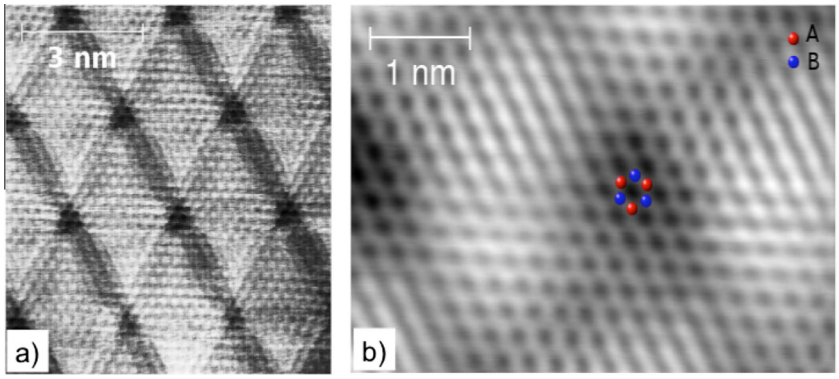

Fig. 5 – STM images of graphene on Ir(111) film acquired setting the following parameters: (a) I = 2 nA, V = 25 mV and (b) I = 2 nA, V = 20 mV. (A color version of this figure can be viewed online.)

the underlying iridium film does not induce deformations to the approximately undoped hexagonal carbon lattice.

Fig. 4 shows Raman spectra taken from graphene on the Ir(111) film (top) and from a zone of the iridium film surface covered by tantalum clips during the graphene growth (bottom). The graphene related spectrum is characterized by a narrow G band at 1610 cm^{-1} and a quasi symmetrical 2D band at 2743 cm^{-1}, whose lineshape can be approximated by a single Lorentzian form [38,39]. The sharp peak at 1555 cm^{-1} in both spectra can be assigned to the vibration of molecular oxygen from air [40]. The origin of the low intensity peaks at 1337 and 1608 cm^{-1} is uncertain at the moment. These bands are also present in the Raman data acquired from a region of the Ir(111) film surface covered by tantalum clips during graphene growth (bottom spectrum) where no graphene related peaks are present. The peak at 1368 cm^{-1} could be assigned to a D peak. When normalized to the O_2 peak, it has the same intensity in both the graphene and the region under the Ta clip. We therefore believe it is not intrinsic to graphene. All spectra were deconvoluted using Lorentzian peak shapes and the ratio between 2D and G band intensity (area) is ~6 indicative of monolayer graphene. This result can be surprising because no Raman for R0 phase was observed on graphene Ir bulk [30]. However, differences in experimental setup and measurement conditions can explain the higher signal-to-noise ratio in our case. We note that the Raman shifts with respect to suspended graphene are larger than that observed by Starodub et al. for R30 graphene [30] which is highlighting the fact we have R0 graphene.

The G and 2D bands in the spectra are upshifted compared to suspended graphene ($\omega_G^0 \sim 1581\ cm^{-1}$ and $\omega_{2D}^0 \sim 2680\ cm^{-1}$) [41], which can be regarded as almost undoped and unstrained, by $\Delta\omega_G \sim 29\ cm^{-1}$ and $\Delta\omega_{2D} \sim 63\ cm^{-1}$ ($\omega_G^{1LG} \sim 1610.4 \pm 0.7\ cm^{-1}$ and $\omega_G^{1LG} \sim 2743.0 \pm 1.6\ cm^{-1}$). Such shifts with $\Delta\omega_{2D}/\Delta\omega_G \sim 2.17$ correspond to changes induced mostly by strain with reported $\Delta\omega_{2D}/\Delta\omega_G$ of 2.4–2.5 [42,43]. On the other hand, the widths of the bands $\Gamma_G^{1LG} = 13.6 \pm 1.6\ cm^{-1}$ and $\Gamma_{2D}^{1LG} = 46.1 \pm 2\ cm^{-1}$ together with $\Delta\omega_{2D}/\Delta\omega_G$ are slightly lower than the ratio for pure strain indicating a minor level of doping [44] due to air exposure. The changes in G and 2D band frequencies associated with small doping levels (both n- and p-doping) can be approximated by a linear fit with $\Delta\omega_{2D}/\Delta\omega_G$ of ~0.5 [44,45]. From the above, we obtain contributions of pure strain to the measured shifts $\Delta\omega_G(\varepsilon) \sim 25\ cm^{-1}$ and $\Delta\omega_{2D}(\varepsilon) = 61\ cm^{-1}$. From the values of the shift we can calculate the compressive strain of 0.44% [42,46,47]. The compression can be readily expected due to the opposite thermal expansion coefficients (TEC) of graphene and its substrate causing compressive strains upon cooling after graphene growth [48,49]. It should be noted that in our case the TEC mismatch is driven by silicon instead of iridium because of the small thickness of Ir layer [22]. The theoretical compression level in graphene should be then close to 1% considering the TEC values of silicon [50] and graphene [51]. The smaller measured compression indicates slipping of graphene at the interface and/or the formation of wrinkles. The presence of the latter can be deduced from the widths of the Raman bands. The 2D band in monolayer graphene broadens as a result of both doping [44] and wrinkling [46], while the G band narrows as a result of doping [44] and broadens as a result of wrinkling [46]. The experimental widths of ~14 and 46 cm^{-1} for the G and 2D bands, respectively, might hence correspond to the combination of the two effects. It should be mentioned that the broadening might be induced also by non-uniform strain fields besides the wrinkles, which go often hand in hand in such systems [45,52]. Finally, we do not assume 2D band broadening due to an increased disorder, since no intense D band around 1360–1370 cm^{-1} can be detected from Fig. 4 in the graphene spectrum in comparison to the Raman spectrum of the substrate region covered by the Ta clip during graphene growth. Hence, we conclude a very low density of defects in the hexagonal pattern of graphene.

The STM images reported in Fig. 5 demonstrate the honeycomb lattice of the graphene layer after air exposure and annealing in UHV condition. Graphene sheets have been found in different areas of the sample where large terraces of Ir surface extend up to 100 nm. The sheets are characterized by Moiré superstructure (Fig. 5 (a)) in analogy to the behaviour of graphene grown with different methodologies on bulk Ir(111) [53]. The lack of defects highlighted by Raman spectroscopy is confirmed by the atomic-scale image, where the carbon sublattices, composed of A and B carbon atoms, can be clearly seen in the hexagonal pattern. Consequently the symmetry is preserved, inducing a graphene formation characterised by a carbon layer weakly coupled to the underlying iridium. As in the case of Zeller et al. [22], the Moiré pat-

tern related to the slightly different lattice parameters between iridium and graphene structures is present as periodic protrusions, characterised by a superstructure vector of 26.1 ± 0.5 Å: the slightly larger value with respect to that measured for the R0 phase on bulk Ir(111) [30] can be related to thermal expansion coefficients as a consequence of the further higher annealing and subsequent cooling down to room temperature just before acquisition. It should be mentioned that we have always obtained the R0 phase, in contrast to previous reports on the formation of rotated domain at higher CVD temperature [22].

4. Conclusions

We have shown that graphene can be grown on iridium single crystal films preserving the similar electronic and structural properties of graphene grown on bulk iridium crystal. Starting from the XPS data acquired from the C1s core level, a single component appears as in the case of pure graphene. Indeed, following the NEXAFS spectra we have obtained a highly ordered carbon sheet lying almost planar on the Ir film surface. ARPES data exhibit the electronic band structure of a single graphene layer, essentially unperturbed by the electronic states of the substrate. The high resolution STM images are free of atomic-scale defects and endorse the presence of a weak coupling to the substrate. Both carbon sub-lattices are noticeable in microscopy images indicating an unbroken symmetry. The Moiré diffraction pattern, Dirac cone analysis, and Raman spectroscopy confirm the good quality of graphene monolayer: homogeneity and lack of defects are the predominant features. In addition, the alternative precursor molecules used for the CVD growth yield similar results.

This route of synthesis on inexpensive substrates can be upscaled, and Ir/YSZ/Si(111) wafers of 4 in. diameter are already available. Regarding potential routes to detach and transfer these graphene samples to other substrates, we note that the currently used etching-based methods [4–8] should not be suitable in this case. Ir is a chemically inert noble metal that can be etched only by hot (approx 100 °C) aqua regia (nitro-hydrochloric acid), but nitric acid is also know to react strongly with aromatic carbon surfaces including carbon nanotubes [54]. The recently reported bubbling transfer method [9] seems a more promising way to follow.

Acknowledgements

C.S. and L.P. thank AREA Science Park Trieste and EU-COST Action MP0901 for partial financial support, and D. Lonza and C. Pedersini for technical assistance. A.F., N.V. and A.Grüneis acknowledge a MC-IRSES project (NanoCF) for financial support and the European Community-FP7 CALIPSO (n.312284) Transnational Access Program for supporting their stay at the BESSY and at the Elettra synchrotrons. A.N. and C.W. acknowledge funding from the "Science and Technology of Nanosystems" Programme (Project No. 431103-Molecular Building Blocks/Supramolecular Networks). M.K. and O.F. acknowledge the support from the Czech Grant agency (P208/12/1062). M.W. and M.S. thank DFG Priority Program 1459 "Graphene". G.D.S., M.P. and A.G. acknowledge FIRB Projects RBAP11C58Y and RBFR10DAK6.

Appendix A. Supplementary data

Supplementary data associated with this article can be found, in the online version, at http://dx.doi.org/10.1016/j.carbon.2014.09.045.

REFERENCES

[1] Bonaccorso F, Sun Z, Hasan T, Ferrari AC. Graphene photonics and optoelectronics. Nat Photonics 2010;4:611–22.
[2] Sun S, Gao L, Liu Y. Enhanced dye-sensitized solar cell using graphene-TiO2 photoanode prepared by heterogeneous coagulation. Appl Phys Lett 2010;96:083113.
[3] Park H, Brown PR, Bulović V, Kong J. Graphene as transparent conducting electrodes in organic photovoltaics: studies in graphene morphology, hole transporting layers, and counter electrodes. Nano Lett 2012;12:133–40.
[4] Li X, Cai W, An J, Kim S, Nah J, Yang D, et al. Large-area synthesis of high-quality and uniform graphene films on copper foils. Science 2009;324:1312–4.
[5] Kim KS, Zhao Y, Jang H, Lee SY, Kim JM, Kim KS, et al. Large-scale pattern growth of graphene films for stretchable transparent electrodes. Nature 2009;457:706–10.
[6] Kato T, Hatakeyama R. Direct growth of doping-density-controlled hexagonal graphene on SiO2 substrate by rapid-heating plasma CVD. ACS Nano 2012;6:8508–15.
[7] Scardamaglia M, Aleman B, Amati M, Ewels C, Pochet P, Reckinger N, et al. Nitrogen implantation of suspended graphene flakes: annealing effects and selectivity of sp^2 nitrogen species. Carbon NY 2014;73:371–81.
[8] Bae S, Kim H, Lee Y, Xu X, Park J-S, Zheng Y, et al. Roll-to-roll production of 30-inch graphene films for transparent electrodes. Nat Nanotechnol 2010;5:574–8.
[9] Gao L, Ren W, Xu H, Jin L, Wang Z, Ma T, et al. Repeated growth and bubbling transfer of graphene with millimetre-size single-crystal grains using platinum. Nat Commun 2012;3:699.
[10] Wang B, Bocquet M-L, Marchini S, Günther S, Wintterlin J. Chemical origin of a graphene moiré overlayer on Ru(0001). Phys Chem Chem Phys 2008;10:3530–4.
[11] Sutter P, Hybertsen MS, Sadowski JT, Sutter E. Electronic structure of few-layer epitaxial graphene on Ru(0001). Nano Lett 2009;9:2654–60.
[12] Sutter E, Acharya DP, Sadowski JT, Sutter P. Scanning tunneling microscopy on epitaxial bilayer graphene on ruthenium (0001). Appl Phys Lett 2009;94:133101.
[13] Sutter PW, Flege J-I, Sutter EA. Epitaxial graphene on ruthenium. Nat Mater 2008;7:406–11.
[14] Grüneis A, Kummer K, Vyalikh DV. Dynamics of graphene growth on a metal surface: a time-dependent photoemission study. New J Phys 2009;11:073050.
[15] Addou R, Dahal A, Batzill M. Growth of a two-dimensional dielectric monolayer on quasi-freestanding graphene. Nat Nanotechnol 2013;8:41–5.
[16] Haberer D, Vyalikh DV, Taioli S, Dora B, Farjam M, Fink J, et al. Tunable band gap in hydrogenated quasi-free-standing graphene. Nano Lett 2010;10:3360–6.
[17] Lacovig P, Pozzo M, Alfè D, Vilmercati P. Growth of dome-shaped carbon nanoislands on Ir(111): the intermediate between carbidic clusters and quasi-free-standing graphene. Phys Rev Lett 2009;103:166101.

[18] Preobrajenski AB, Ling MN, Vinogradov AS, Martensson N. Controlling graphene corrugation on lattice-mismatched substrates. Phys Rev B 2008;78:073401.
[19] Gsell S, Fischer M, Brescia R, Schreck M, Huber P, Bayer F, et al. Reduction of mosaic spread using iridium interlayers: a route to improved oxide heteroepitaxy on silicon. Appl Phys Lett 2007;91:061501.
[20] Fischer M, Brescia R, Gsell S, Schreck M, Brugger T, Greber T, et al. Growth of twin-free heteroepitaxial diamond on Ir/YSZ/Si(111). J Appl Phys 2008;104:123531.
[21] Fischer M, Gsell S, Schreck M, Brescia R, Stritzker B. Preparation of 4-inch Ir/YSZ/Si(001) substrates for the large-area deposition of single-crystal diamond. Diam Relat Mater 2008;17:1035–8.
[22] Zeller P, Dänhardt S, Gsell S, Schreck M, Wintterlin J. Scalable synthesis of graphene on single crystal Ir(111) films. Surf Sci 2012;606:1475–80.
[23] Müller F, Sachdev H, Hüfner S, Pollard AJ, Perkins EW, Russell JC, et al. How does graphene grow? Easy access to well-ordered graphene films. Small 2009;5:2291–6.
[24] Gsell S, Fischer M, Bauer T, Schreck M, Stritzker B. Yttria-stabilized zirconia films of different composition as buffer layers for the deposition of epitaxial diamond/Ir layers on Si(001). Diamond Relat. Mater. 2006;15:479–85.
[25] Gsell S, Fischer M, Schreck M, Stritzker B. Epitaxial films of metals from the platinum group (Ir, Rh, Pt and Ru) on YSZ-buffered Si(111). J Cryst Growth 2009;311:3731–6.
[26] Nefedov A, Wöll C. Advanced application of NEXAFS spectroscopy for functionalized surfaces, in surface science techniques. In: Bracco G, Holst B, editors. Springer Series in Surface Science, 51. Heidelberg: Springer-Verlag; 2013. p. 277–303.
[27] Pacilé D, Papagno M, Rodríguez A, Grioni M, Papagno L, Girit Ç, et al. Near-edge X-ray absorption fine-structure investigation of graphene. Phys Rev Lett 2008;101:066806.
[28] Petaccia L, Vilmercati P, Gorovikov S, Barnaba M, Bianco A, Cocco D, et al. BaD ElPh: a 4m normal-incidence monochromator beamline at Elettra. Nucl Instrum Methods Phys Res A 2009;606:780–4.
[29] Ferrari AC. Raman spectroscopy of graphene and graphite: disorder, electron–phonon coupling, doping and nonadiabatic effects. Solid State Commun 2007;143:47–57.
[30] Starodub E, Bostwick A, Moreschini L, Nie S, El Gabaly F, McCarty KF, et al. In-plane orientation effects on the electronic structure, stability, and Raman scattering of monolayer graphene on Ir (111). Phys Rev B 2011;83:125428.
[31] Trickey SB, Müller-Plathe F, Diercksen GHF, Boettger JC. Interplanar binding and lattice relaxation in a graphite dilayer. Phys Rev B 1992;45:4460–8.
[32] Rosenberg R, Love P, Rehn V. Polarization-dependent C(K) near-edge X-ray-absorption fine structure of graphite. Phys Rev B 1986;33:4034–7.
[33] Kralj M, Pletikosić I, Petrović M, Pervan P, Milun M, N'Diaye AT, et al. Graphene on Ir(111) characterized by angle-resolved photoemission. Phys Rev B 2011;84:075427.
[34] Pletikosić I, Kralj M, Pervan P, Brako R, Coraux J, N'Diaye A. Dirac cones and minigaps for graphene on Ir(111). Phys Rev Lett 2009;102:056808.
[35] N'Diaye AT, Coraux J, Plasa TN, Busse C, Michely T. Structure of epitaxial graphene on Ir(111). New J Phys 2008;10:043033.
[36] Haberer D, Petaccia L, Fedorov AV, Praveen CS, Fabris S, Piccinin S, et al. Anisotropic Eliashberg function and electron–phonon coupling in doped graphene. Phys Rev B 2013;88:081401.
[37] Fedorov AV, Verbitskiy NI, Haberer D, Struzzi C, Petaccia L, Usachov D, et al. Observation of a universal donor-dependent vibrational mode in graphene. Nat Commun 2014;5:3257.
[38] Ferrari AC, Meyer JC, Scardaci V, Casiraghi C, Lazzeri M, Mauri F, et al. Raman spectrum of graphene and graphene layers. Phys Rev Lett 2006;97:187401.
[39] Frank O, Mohr M, Maultzsch J, Thomsen C, Riaz I, Jalil R, et al. Raman 2D-band splitting in graphene: theory and experiment. ACS Nano 2011;5:2231–9.
[40] Weber A, McGinnis EA. The Raman spectrum of gaseous oxygen. J Mol Spectrosc 1960;4:195–200.
[41] Berciaud S, Li X, Htoon H, Brus LE, Doorn SK, Heinz TF. Intrinsic line shape of the Raman 2D-mode in freestanding graphene monolayers. Nano Lett 2013;13:3517–23.
[42] Filintoglou K, Papadopoulos N, Arvanitidis J, Christofilos D, Frank O, Kalbac M, et al. Raman spectroscopy of graphene at high pressure: effects of the substrate and the pressure transmitting media. Phys Rev B 2013;88:045418.
[43] Lee JE, Ahn G, Shim J, Lee YS, Ryu S. Optical separation of mechanical strain from charge doping in graphene. Nat Commun 2012;3:1024.
[44] Kalbac M, Reina-Cecco A, Farhat H, Kong J, Kavan L, Dresselhaus MS. The influence of strong electron and hole doping on the Raman intensity of chemical vapor-deposition graphene. ACS Nano 2010;4:6055–63.
[45] Frank O, Vejpravova J, Holy V, Kavan L, Kalbac M. Interaction between graphene and copper substrate: the role of lattice orientation. Carbon NY 2014;68:440–51.
[46] Frank O, Tsoukleri G, Parthenios J, Papagelis K, Riaz I, Jalil R, et al. Compression behavior of single-layer graphenes. ACS Nano 2010;4:3131–8.
[47] Zabel J, Nair RR, Ott A, Georgiou T, Geim AK, Novoselov KS, et al. Raman spectroscopy of graphene and bilayer under biaxial strain: bubbles and balloons. Nano Lett 2012;12:617–21.
[48] Hattab H, N'Diaye AT, Wall D, Klein C, Jnawali G, Coraux J, et al. Interplay of wrinkles, strain, and lattice parameter in graphene on iridium. Nano Lett 2012;12:678–82.
[49] Tapasztó L, Dumitrică T, Kim SJ, Nemes-Incze P, Hwang C, Biró LP. Breakdown of continuum mechanics for nanometre-wavelength rippling of graphene. Nat Phys 2012;8:739–42.
[50] Touloukian YS, Kirby RK, Taylor RE, Lee TYR. Thermal expansion – nonmetallic solids, thermophysical properties of matter. New York: IFI/Plenum; 1977. 13.
[51] Yoon D, Son Y-W, Cheong H. Negative thermal expansion coefficient of graphene measured by Raman spectroscopy. Nano Lett 2011;11(8):3227–31.
[52] He R, Zhao L, Petrone N, Kim KS, Roth M, Hone J, et al. Large physisorption strain in chemical vapor deposition of graphene on copper substrates. Nano Lett 2012;12:2408–13.
[53] Coraux J, T N'Diaye A, Engler M, Busse C, Wall D, Buckanie N, et al. Growth of graphene on Ir(111). New J Phys 2009;11:023006.
[54] Dreyer DR, Park S, Bielawski CW, Ruoff RS. The chemistry of graphene oxide. Chem Soc Rev 2010;39:228.